Control of the threonine-synthesis pathway in *Escherichia coli*: a theoretical and experimental approach

Christophe CHASSAGNOLE*, David A. FELL*†, Badr RAÏS*, Bernard KUDLA‡ and Jean-Pierre MAZAT*[1]

*INSERM EMI 9929, University Victor Segalen Bordeaux 2, 146 rue Léo Saignat, 33076 Bordeaux, France, †School of Biological and Molecular Sciences, Oxford Brookes University, Oxford OX3 0BP, U.K., and ‡52 rue de Gometz, 91470 Les Molières, France

A computer simulation of the threonine-synthesis pathway in *Escherichia coli* Tir-8 has been developed based on our previous measurements of the kinetics of the pathway enzymes under near-physiological conditions. The model successfully simulates the main features of the time courses of threonine synthesis previously observed in a cell-free extract without alteration of the experimentally determined parameters, although improved quantitative fits can be obtained with small parameter adjustments. At the concentrations of enzymes, precursors and products present in cells, the model predicts a threonine-synthesis flux close to that required to support cell growth. Furthermore, the first two enzymes operate close to equilibrium, providing an example of a near-equilibrium feedback-inhibited enzyme. The predicted flux control coefficients of the pathway enzymes under physiological conditions show that the control of flux is shared between the first three enzymes: aspartate kinase, aspartate semialdehyde dehydrogenase and homoserine dehydrogenase, with no single activity dominating the control. The response of the model to the external metabolites shows that the sharing of control between the three enzymes holds across a wide range of conditions, but that the pathway flux is sensitive to the aspartate concentration. When the model was embedded in a larger model to simulate the variable demands for threonine at different growth rates, it showed the accumulation of free threonine that is typical of the Tir-8 strain at low growth rates. At low growth rates, the control of threonine flux remains largely with the pathway enzymes. As an example of the predictive power of the model, we studied the consequences of over-expressing different enzymes in the pathway.

Key words: amino acid, biosynthetic pathway modelling, computer simulation, metabolic control analysis, metabolic engineering.

INTRODUCTION

The goal of metabolic engineering is the rational design and implementation of changes in an organism's properties to alter its metabolism in the desired manner [1]. One particular area of interest is the possibility of increasing rates and yields of amino acid synthesis by micro-organisms. However, in strains where conventional mutation and selection have already led to high productivity, it has proved difficult both to determine exactly what the critical changes have been and to design strategies for further improvement [2].

The reasons for this have been explored theoretically, particularly through the theory of metabolic control analysis, which has given reasons for doubting that large increases in flux could generally be obtained simply by abolishing feedback inhibition [3] or over-expressing a single pathway enzyme [3–6]. These basic propositions have been confirmed experimentally (e.g. [7,8]). If over-expression of a single enzyme is to be effective, then according to metabolic control analysis [9–13] the enzyme must be one with a significant flux-control-coefficient value [4,6], the factor relating a fractional change in flux to a small change in enzyme activity. One strategy for identifying potential targets for over-expression is therefore to determine the flux control coefficients of the enzymes in the metabolic pathway and then to choose the one with the largest coefficient value. If this enzyme is over-expressed, then inevitably its flux control coefficient falls and the flux control coefficient of one or more of the other enzymes rises, so that another point in the pathway becomes a more significant focus for further action. A theoretical method for identifying a set of linked changes on the basis of control analysis has been proposed [14], and there are experimental examples where it was necessary to change the activities of several enzymes to maximize the flux change, sometimes including ones that initially had negligible influence on the pathway flux [7,8,15].

An alternative suggestion, Kacser and Acerenza's Universal Method [5], is that only the co-ordinate over-expression of sets of enzymes in precise ratios can achieve very large flux changes without disruption of metabolism. In fact, this is seen where selection of high-producing strains has yielded micro-organisms with de-repressed operons for a particular pathway, such as the *Escherichia coli* threonine-producing strain Tir-8, or multiple copies of the pathway genes, as in commercial penicillin-producing strains. However, reasons for not favouring this approach are that it can be very difficult to genetically modify an organism so that large numbers of proteins are co-ordinately over-expressed, and there is the possibility that yields may be reduced by the increased burden of protein synthesis. If the other methods, involving more targeted over-expression informed by control analysis, could be nearly as effective, as theory suggests [3,16], they would be preferable.

All this implies that engineered increases in pathway flux require quantitative tools to identify the required changes. This can involve approaches including experimental control analysis of the pathway [10,11], metabolic design analysis [16] or modelling. Models can include dynamic computer models and theoretical control-analysis models [14,17]. In the former case, it is still necessary to determine the sensitivity of the pathway flux to the parameters of the model, which is formally equivalent to a metabolic control analysis of the flux control coefficients of the

[1] To whom correspondence should be addressed (e-mail JP.Mazat@phys-mito.u-bordeaux2.fr).

pathway parameters. In spite of the interest in engineering amino acid synthesis, the only recently reported models are of the lysine pathway in *Corynebaterium glutamicum* [18] and the tryptophan pathway in *C. glutamicum* and *E. coli* [19].

It is for these reasons that in the previous two papers [20,21] we have described the experimental measurements that have formed the basis for the development of the model of *E. coli* threonine synthesis described here. The model functions in two ways: it can predict the time course of threonine synthesis for particular levels of enzymes and intermediates of central metabolism, and it can predict the flux control coefficients of the enzymes under a range of intracellular conditions different from those of the original measurements.

MATERIALS AND METHODS

Experimental

All chemicals, the preparation of crude extract and the enzyme assays are described in the accompanying papers [20,21].

Intracellular measurements

Amino acids

The amino acid extractions and quenching were performed as described in [22]. In order to stop metabolism, 200 ml of culture medium was passed through a 0.2 μm-pore-size filter (Durapore, Millipore) and the filter was then put in 70 % ethanol for 30 min after vigorous vortex agitation at room temperature. After centrifugation at 13000 ***g*** for 20 min, the supernatant was filtered through a 45 mm-diameter, 0.2 μm filter (Millipore). The amino acid concentrations were determined by HPLC, using a pre-column derivation with OPA (*o*-phthaldehyde-thiol). They were analysed on a Hypersil ODS (250 mm × 4.6 mm) 5 μm column in reverse phase with a concentration gradient formed from potassium acetate buffer according to Joseph and Marsden [23].

Adenylate nucleotides

Nucleotide extraction and quenching were started by adding perchloric acid at 4 % (w/v), final concentration, and incubating at −25 °C for 10 min. After thawing the solution at 0 °C and centrifugation for 10 min at 10000 ***g***, the supernatant was neutralized to a final pH of 7.8 with 2 M KOH/0.2 M Mops. After incubating for 10 min to allow protein precipitation, the solution was centrifuged for 10 min at 10000 ***g*** and the supernatant filtered with a 0.2 μm filter (Millipore). The ATP had to be measured immediately due to its instability. The ATP and ADP concentrations were determined by the luciferin/luciferase reaction [24,25] with a microstrip luminescence biometer (Luminoskan, Labsystem France S.A.). For ATP and ADP determinations, the reaction mixture contained, in five different 300 μl microcuvettes, 100 μl of assay buffer (25 mM Hepes/15 mM KOH/10 mM $MgSO_4$/1.5 mM phosphoenolpyruvate/11.5 units/l pyruvate kinase), 10 μl of sample and 20 μl of ADP standard in a range of 0–20 pmol/microcuvette. These mixtures were incubated at room temperature for 15 min to allow the complete transformation of ADP to ATP. The measurement was then started by an automatic 100 μl injection of the measurement mixture from the ATP bioluminescence assay kit HS II (Boehringer-Mannheim). An internal-standard solution was used to avoid quenching problems due to the sample and to correct for any incomplete transformation of ADP.

Pyridine nucleotides

Acid extraction of the oxidized nucleotide and basic extraction of the reduced nucleotide were performed as described in [26]. The measurement was made using a spectrophotometric cycling assay for signal amplification [26]. This very sensitive method of analysis was necessary to avoid a biomass concentration that could cause loss of the analyte [27].

Intracellular volume

The bacterial intracellular volume was estimated from measured media osmolarities, using a calibration curve [28].

Theoretical methods

Model structure

The full system that we simulated is shown in Figure 1, which includes reactions for threonine consumption that were only included in certain simulations. In many cases the simulations treated threonine as an end-product at a fixed concentration. The

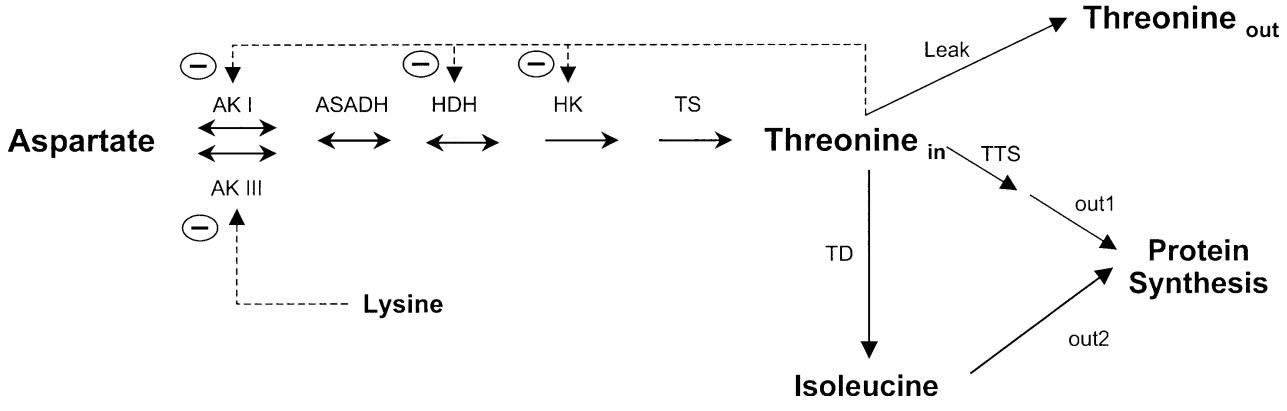

Figure 1 Model of threonine metabolism

The scheme shows the full model of threonine synthesis and utilization. Subsets of this scheme were used for certain simulations, as described in the text and Table 1. out1 and out2 refer to the incorporation of threonine and isoleucine into protein. AK, aspartate kinase; ASADH, aspartate semialdehyde dehydrogenase; HDH, homoserine dehydrogenase; HK, homoserine kinase; TS, threonine synthase; TD, threonine deaminase; TTS, threonyl-tRNA synthetase.

Table 1 The dynamic system: ordinary differential equations of the simulated system shown in Figure 1

v_i refers to the rate of the process i computed with the appropriate function as described in the text and with the current values of the metabolite concentrations. All simulations included reactions 2–5, and steady-state solutions of the *in vivo* pathway to threonine included only these processes. Dynamic simulations of the *in vitro* dynamics system included in addition equations 1 and 9–11. Simulations of the steady state with threonine demand at variable growth rates used processes 2–8. out1 and out2 refer to the incorporation of threonine and isoleucine into protein; leak refers to the loss of threonine through the cell wall; endo indicates the loss of NADPH represented by eqn (1). AK, aspartate kinase; ASD, aspartate semialdehyde dehydrogenase; TS, threonine synthase; TD, threonine deaminase; TTS, threonyl-tRNA synthetase; HK, homoserine kinase; HDH, homoserine dehydrogenase; aspp, β-aspartyl phosphate. The primes denote the derivatives with respect to time.

Process no.	Metabolite derivative	Equation
1	Aspartate′	$= -v_{AK}$
2	aspp′	$= v_{AK} - v_{ASD}$
3	Aspartate β-semialdehyde′	$= v_{ASD} - v_{HDH}$
4	Homoserine′	$= v_{HDH} - v_{HK}$
5	*O*-Phospho-homoserine′	$= v_{HK} - v_{TS}$
6	Threonine′	$= v_{TS} - v_{TD} - v_{TTS} - v_{leak}$
7	Isoleucine′	$= v_{TD} - v_{out2}$
8	Threonyl-tRNA′	$= v_{TTS} - v_{out1}$
8a	tRNA′	$= -v_{TTS} + v_{out1}$
9	ATP′	$= -v_{AK} - v_{HK} - v_{ATPase}$
9a	ADP′	$= v_{AK} + v_{HK} + v_{ATPase}$
10	NADPH′	$= -v_{ASD} - v_{HDH} - v_{endo}$
10a	$NADP^{+\prime}$	$= v_{ASD} + v_{HDH} + v_{endo}$
11	P_i'	$= v_{ASD} + v_{TS} + v_{ATPase}$

Table 2 Parameters of the model

aspp, β-aspartyl phosphate; hsp, *O*-phospho-homoserine; ASA, aspartic β-semialdehyde; α, the partial inhibition coefficient. For enzyme abbreviations see Table 1.

Enzyme	K_m (mM)	Inhibition	K_{eq}
AK I	Aspartate, 0.97 ± 0.48 ATP, 0.98 ± 0.5 aspp, 0.017 ± 0.004 ADP, 0.25	K_{iThr}, 0.167 ± 0.003 mM h_{Thr}, 4.09 ± 0.26 α, 2.47 ± 0.17	6.4×10^{-4}
AK III	Aspartate, 0.32 ± 0.08 ATP, 0.22 ± 0.02 aspp, 0.017 ± 0.004 ADP, 0.25	K_{iLys}, 0.391 ± 0.08 mM h_{Lys}, 2.8 ± 1.4	6.4×10^{-4}
ASD	aspp, 0.022 ± 0.001 NADPH, 0.029 ± 0.002 ASA, 0.11 ± 0.008 $NADP^+$, 0.144 ± 0.02 P_i, 10.2 ± 1.4		2.84×10^5
HDH	ASA, 0.24 ± 0.03 NADPH, 0.037 ± 0.006 Homoserine, 3.39 ± 0.33 $NADP^+$, 0.067 ± 0.006	K_{iThr}, 0.097 mM h, 1.41 α, 3.93	1×10^{11} M^{-1}
HK	Homoserine, 0.11 ATP, 0.072	K_{iThr}, 1.09 mM K_{iLys}, 9.45 mM $K_{ihomoserine}$, 4.7 mM K_{iATP}, 4.35 mM	
TS	hsp, 0.31 ± 0.03		
TTS	Threonine, 0.5 tRNA, 0.12		
TD	Threonine, 1.3	K_{ille}, 0.002 mM	

overall equations of the full dynamic system are listed in Table 1; terms related to threonine utilization only appear in simulations that explicitly include this, and the equations for NADPH, ATP and aspartate are only simulated when modelling the cell-free synthesis.

Table 3 Specific activities of the enzymes of the threonine-synthesis pathway in cell-free extracts of *E. coli* used for the simulations

The values in the first two columns under Activity are the means ± range of two estimates, except for threonine synthase, where the S.E.M.s of three determinations are given. In the third column under Activity, the results are the means ± S.E.M. for nine cultures, each measured twice.

	Activity (nmol · min^{-1} · mg^{-1})		
Enzyme	*In vitro*, aspartate variable	*In vitro*, threonine variable	*In vivo*
Aspartate kinase I	402 ± 18	497 ± 17	463 ± 26
Aspartate kinase III	283 ± 8	319 ± 2	299 ± 19
Aspartate semialdehyde dehydrogenase	526 ± 16	583 ± 36	598 ± 22
Homoserine dehydrogenase	2292 ± 32	3520 ± 89	2585 ± 206
Homoserine kinase	356 ± 7	438 ± 8	483 ± 42
Threonine synthase	161 ± 4	187 ± 4	208 ± 13

Table 4 Measured metabolite concentrations used for simulating the *in vivo* steady state

The values for amino acids are the means from two measurements on one culture, the adenine nucleotides the means of three measurements on one culture, and the pyridine nucleotides the means of triplicate determinations on two cultures. All errors represent S.E.M.

Metabolite	Content (nmol · g of dry $weight^{-1}$)	Concentration (mM)
Aspartate	2854 ± 67	1.34 ± 0.03
Threonine	7444 ± 144	3.49 ± 0.07
Lysine	984 ± 23	0.46 ± 0.01
ATP	2792 ± 43	1.31 ± 0.021
ADP	352 ± 6	0.17 ± 0.003
$NADP^+$	1341 ± 95	0.63 ± 0.041
NADPH	1197 ± 73	0.56 ± 0.033
P_i	Not determined	5

Pathway enzymes to threonine

The development of the enzyme rate expressions and the measurement of their parameters has been described in the first paper of this series [20]. Except where otherwise stated, the simulations reported here use those values (see Table 2). Again, it is worth emphasizing that the rate equations used for the simulation are accurate for metabolite concentrations within the physiological range, not for all possible combinations of concentrations from zero to saturating, and represent the effects of products, both as inhibitors because of their binding at the active site in competition with the substrates, and, when appropriate, as substrates of the reverse reaction.

The simulations of the experiments on cell-free synthesis of threonine used the measured specific activities and protein concentration of the extract used for the corresponding experiment (Table 3) together with the relevant initial metabolite concentrations (Table 4). For the simulations of the pathway under *in vivo* conditions, the enzyme activities used were the average values measured in extracts of *E. coli* Tir-8 and given in Table 3. The concentrations of metabolites external to the pathway (e.g. NADPH and ATP) were taken from measurements made on extracts of growing cells of the strain used here (Table 4).

Other reactions

The control experiments on threonine synthesis in cell-free extracts [21] established that, in the absence of other substrates, the extract catalysed a slow loss of NADPH at a rate proportional to the concentration of NADPH. Accordingly, when modelling the *in vitro* synthesis of threonine, we represented this reaction by the empirical equation:

$$v = k_{\mathrm{NADPH}} \cdot [\mathrm{protein}] \cdot [\mathrm{NADPH}] \quad (1)$$

derived previously [21] with $k_{\mathrm{NADPH}} = 0.0054\ \mathrm{ml \cdot mg^{-1} \cdot min^{-1}}$. The extracts were also observed to have a slow ATPase activity in the absence of threonine synthesis, zero order in ATP and first order in protein. The rate constant k_{ATP} was estimated [21] as $0.064\ \mathrm{ml \cdot mg^{-1} \cdot mM \cdot min^{-1}}$.

Extension of the model to represent growth-dependent threonine demand

To assess the extent to which the threonine-pathway model described above can be applied to predicting responses of the whole cell, it was decided to extend it to create a demand for threonine. (Ideally, it should also be extended to represent the demand the pathway makes on its precursors, but even at stimulated pathway rates this will still not represent a very large proportion of their turnover.) Three elements of the demand for threonine were modelled: the withdrawal of threonine for protein synthesis during growth; the further metabolism of threonine to isoleucine, which was then itself withdrawn for protein synthesis; and a leak of threonine out of the cell by diffusion, corresponding to the production of free threonine by *E. coli* Tir-8 (Figure 1). If every one of these processes were to be represented by a zero-order reaction, then control would always reside in these demand steps and there would be no variation in the partitioning of the flux between them. Hence, the incorporation of threonine into protein was represented by the threonyl-tRNA synthetase reaction, a two-substrate enzyme-catalysed reaction between threonine and its tRNA, forming threonyl-tRNA according to the equation:

$$v = \frac{V_{\mathrm{m}} \dfrac{[\mathrm{Thr}]}{K_{\mathrm{Thr}}} \cdot \dfrac{[\mathrm{tRNA}]}{K_{\mathrm{tRNA}}}}{\left(1 + \dfrac{[\mathrm{Thr}]}{K_{\mathrm{Thr}}}\right)\left(1 + \dfrac{[\mathrm{tRNA}]}{K_{\mathrm{tRNA}}}\right)} \quad (2)$$

The K_{Thr} value was set at 0.5 mM, some five or six times higher than reported values for the enzyme, and the K_{tRNA} value at 0.12 mM, again a high estimate. The values were chosen to give steady states with realistic levels of threonine; in any case, the step represents the overall kinetics of the incorporation of threonine into protein and therefore would not be expected to be kinetically identical to the first enzyme of this process. The limiting rate, V_{m}, was set at $0.3\ \mu\mathrm{mol \cdot mg^{-1} \cdot min^{-1}}$, and the total tRNA pool at 0.01 mM. Threonyl-tRNA was incorporated into protein (releasing tRNA) by a zero-order process at a rate that was calculated from the threonine content of *E. coli* biomass of $241\ \mu\mathrm{mol \cdot g\ of\ dry\ weight^{-1}}$ [29], an estimate of soluble cell protein of 150 mg/g of dry weight, and a maximum growth rate of $0.0156\ \mathrm{min^{-1}}$ for wild-type cells growing on glucose [30]. This leads to a maximum utilization rate of $25\ \mathrm{nmol \cdot mg^{-1} \cdot min^{-1}}$ at the maximum growth rate and a proportionately lower rate at lower growth rates.

The withdrawal of threonine for isoleucine synthesis was represented by the first enzyme of the pathway, the biosynthetic threonine deaminase, which was modelled by Michaelis–Menten kinetics with competitive inhibition by isoleucine and a V_{m} of $0.3\ \mu\mathrm{mol \cdot mg^{-1} \cdot min^{-1}}$. Isoleucine utilization for protein synthesis was modelled by a zero-order process, as for threonyl-tRNA incorporation. The maximal rate was set at $28.7\ \mathrm{nmol \cdot mg^{-1} \cdot min^{-1}}$, corresponding to the slightly higher isoleucine content of *E. coli* biomass ($276\ \mu\mathrm{mol \cdot g\ of\ dry\ weight^{-1}}$ [29]).

The rate of passive diffusion of threonine from the cells was assumed to be similar to that measured in *C. glutamicum*, where the first-order rate constant is $0.003\ \mathrm{min^{-1}}$ [31].

Simulation

The model was implemented in the biochemical simulation package SCAMP [32,33]. This allows both dynamic simulations and solutions for steady states, with automated calculation of elasticities and control coefficients as well as other derived parameters. A specimen command file for SCAMP is available from D. A. F. web site (http://bms-mudshark.brookes.ac.uk).

Metabolic control analysis

The analysis of the properties of the model uses the formalism of metabolic control analysis [9,11,12], which defines a number of coefficients to act as measures of the properties of a metabolic network's steady state. In particular, the flux control coefficient ($C^{J_{\mathrm{ydh}}}_{\mathrm{xase}}$) describes the effect of a change in the activity of enzyme xase on a flux J_{ydh} measured through step ydh as:

$$C^{J_{\mathrm{ydh}}}_{\mathrm{xase}} = \frac{\partial J_{\mathrm{ydh}}}{\partial v_{\mathrm{xase}}} \cdot \frac{v_{\mathrm{xase}}}{J_{\mathrm{ydh}}} = \frac{\partial \ln J_{\mathrm{ydh}}}{\partial \ln v_{\mathrm{xase}}} \quad (3)$$

The change in the activity of the enzyme can be brought about by any parameter that acts exclusively on the enzyme in question; the simulation package SCAMP incorporates calculation of control coefficients by numerical differentiation of the steady-state solution with respect to a parameter specified by the user. In this case, we specified the V_{m} of each enzyme as the parameter acting on the activity.

A related coefficient of interest is the response coefficient ($R^{J_{\mathrm{ydh}}}_{P}$) [9,11], which quantifies the change in any variable (including flux) of the metabolic system to any parameter P other than enzyme activity. The definition is similar to that of the flux control coefficient:

$$R^{J_{\mathrm{ydh}}}_{P} = \frac{\partial J_{\mathrm{ydh}}}{\partial P} \cdot \frac{P}{J_{\mathrm{ydh}}} = \frac{\partial \ln J_{\mathrm{ydh}}}{\partial \ln P} \quad (4)$$

If P is an external effector that acts on the flux J_{ydh} through the pathway enzyme xase, the response coefficient for the effect of P is composed of the flux control coefficient with respect to xase and an elasticity coefficient ($\epsilon^{\mathrm{xase}}_{P}$) of xase with respect to P that measures the local kinetic response of the enzyme:

$$R^{J_{\mathrm{ydh}}}_{P} = C^{J_{\mathrm{ydh}}}_{\mathrm{xase}}\, \epsilon^{\mathrm{xase}}_{P} \quad (5)$$

Again, the response coefficients reported here were computed by SCAMP for user-specified effectors.

The elasticity coefficient that appears in the equation for the response coefficient is defined for the effect of metabolite S on the velocity v of enzyme xase as the fractional change in rate of the isolated enzyme for a fractional change in substrate S, with all other effectors of the enzyme held constant at the values they have in the metabolic pathway:

$$\epsilon^{\mathrm{xase}}_{S} = \frac{\partial v_{\mathrm{xase}}}{\partial S} \cdot \frac{S}{v_{\mathrm{xase}}} = \frac{\partial \ln |v_{\mathrm{xase}}|}{\partial \ln S} \quad (6)$$

Although the flux control coefficient predicts the change in flux in a pathway in response to a small change in enzyme activity, it

cannot be used for very large changes in enzyme activity caused by over-expression of an enzyme, since the flux control coefficient itself changes with enzyme activity. Small and Kacser [4] derived the following approximate expression for estimating the factor f by which the pathway flux J will increase for an r-fold increase in the amount of enzyme activity E in a linear pathway:

$$f = \frac{1}{1 - \frac{r-1}{r} C_E^J} \quad (7)$$

Although this approximation is not necessary when a model is available to make a more precise calculation of the effect of changes in enzyme activity, we have assessed its validity for the threonine-synthesis pathway by comparing the predictions with the results from the model.

RESULTS AND DISCUSSION

Simulation of cell-free threonine-synthesis dynamics

The experiments on cell-free synthesis of threonine were used to test the model, since the ability to reproduce dynamic experiments is a more stringent test than reproducing steady-state concentrations *in vivo*. The initial model that was compared with the cell-free experiments used the kinetic parameters found experimentally without adjustment and the equations described above, except that aspartate inhibition of homoserine dehydrogenase was not included. Although the simulations reproduced the main features of the experiments in terms of intermediate concentrations and approximate time course (results not shown), there were three problems. First, the amounts of NADPH consumed and threonine formed by the end of the experiments were not predicted with sufficient accuracy in all of the experiments. Secondly, the predicted consumption of ATP was generally too high, particularly towards the end of the incubation when the threonine flux was low. Thirdly, the concentrations predicted for homoserine and *O*-phospho-homoserine were too high, and the accumulation of this amount of the intermediate was delaying the appearance of threonine relative to the experiments.

Accordingly, we modified the model as follows. The first change was to the equilibrium constant of aspartate semialdehyde dehydrogenase, since the asymptotic levels of threonine and NADPH appeared to be most sensitive to this parameter. This was because the enzyme was approaching equilibrium near the end of the time course on account of the accumulation of its product phosphate formed by the hydrolysis of ATP. By trial and error, a value of 1.78×10^6 was found to be suitable, which was higher than our experimentally determined value (Table 2 and [20]), but still lower than the previously published value [34]. The second change related to the endogenous consumption of ATP by the extract, where it seemed that the experimental measurement in the absence of the other metabolites and net threonine synthesis appeared to be an over-estimate in their presence. A reduction of k_{ATP} of about one-third to a value of $0.041\ ml \cdot mg^{-1} \cdot mM \cdot min^{-1}$ improved the fit. Finally, in an attempt to decrease the transient peak of homoserine and *O*-phospho-homoserine we introduced the weak inhibition of homoserine dehydrogenase by aspartate, as reported in [35].

The results of simulation of the revised model are compared with the experiments in Figure 2. As can be seen, for different initial aspartate and threonine concentrations, the values of aspartate, ATP, threonine and NADPH at the end of the incubation are predicted well. The initial rates of consumption of aspartate, ATP and NADPH are modelled well except in the experiment with 2 mM threonine (Figure 2f), and aspartate and NADPH consumption diverge from the observations after 5 min in the experiment with an initial level of 0.5 mM threonine (Figure 2e). In most cases, the synthesis of threonine in the model lags behind its appearance in the experiments; however, the matches between the observed and simulated sums of *O*-phospho-homoserine and threonine are generally better, so there appears to be a slight discrepancy in the balance between the first four enzymes of the pathway and threonine synthase. We would like to stress that, in Figure 2, the same model with a single set of parameter values has been used to fit all the experiments taken from Figures 2 and 3 of our previous paper [21], even though these were performed with two different preparations of the crude extract, which adds to the difficulty of getting all the curves to pass through all the experimental points with common parameters.

Simulation of threonine synthesis under conditions *in vivo*

If it is assumed that the concentrations of the inputs (aspartate, ATP and NADPH) and the outputs (threonine, ADP, $NADP^+$ and phosphate) of the pathway are maintained constant by other metabolic processes in the bacterial cell, it is possible to determine whether the rate equations and parameters of the enzymes derived from the previous section predict a steady state for the threonine-synthesis pathway. In performing this simulation, it is not necessary to include either the hydrolysis of ATP or the oxidation of NADPH that are not coupled to threonine synthesis. The inputs and outputs of the pathway are set constant at *in vivo* values that were measured in assays of cell-free extracts from the same cell strain used for measuring the kinetics. The values are given in Table 4 as $nmol \cdot g\ of\ dry\ weight^{-1}$, and are converted into *in vivo* concentrations using the value of intracellular fluid per g of dry weight of cells reported in [28] for a measured medium osmotic strength of 0.2275 osM.

SCAMP was used to solve for a steady state the differential equations derived from the kinetic equations of the five steps of the synthesis pathway. The resulting simulated steady state was characterized by the following concentrations of metabolites: β-aspartyl phosphate, 0.0045 mM; aspartic β-semialdehyde, 0.027 mM; homoserine, 0.037 mM and *O*-phospho-homoserine, 0.041 mM. The steady-state pathway flux to threonine was predicted to be $28\ nmol \cdot min^{-1} \cdot mg\ of\ protein^{-1}$; this compares with the demand for threonine and isoleucine at maximum growth rate calculated in the Materials and methods section as $54\ nmol \cdot min^{-1} \cdot mg\ of\ protein^{-1}$. Hence the simulated synthesis flux is approximately adequate to support growth of the bacterium. In fact, the growth rate of the strain used here is more typically $0.35\ h^{-1}$ (reducing the requirement to $20\ nmol \cdot min^{-1} \cdot mg\ of\ protein^{-1}$), and it is probable that the extraction of the pathway enzymes from the insoluble cell material is not complete. On the other hand, the requirement to make lysine and methionine will demand a greater flux in the upper part of the threonine synthesis pathway, as will the production of excess extracellular threonine.

The prediction of the steady-state concentration of β-aspartyl phosphate (0.0045 mM) is interesting, as it had been too low for us to determine it experimentally in cell extracts. From this and the other simulated concentrations, it is possible to determine the disequilibrium ratios at each enzymic step (i.e. the mass action ratios divided by the equilibrium constants). These were calculated directly and reported by SCAMP as being 0.67, 0.6 and 4.8×10^{-4} for aspartate kinase, aspartate semialdehyde dehydrogenase and homoserine dehydrogenase respectively. By all usual

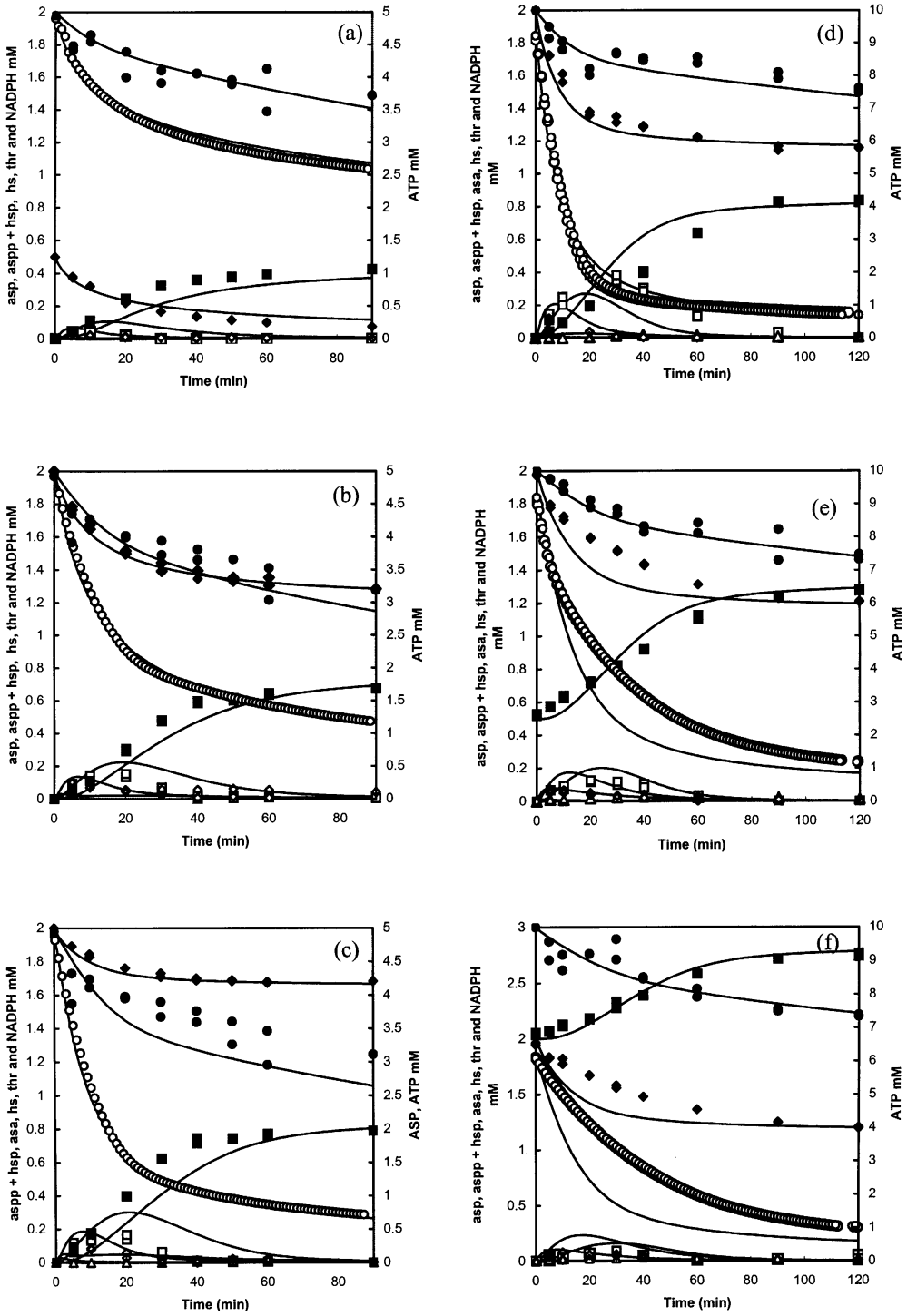

Figure 2 Simulation of cell-free synthesis experiments

The experimental points were taken from Figures 2 and 3 in [21]. The differential system shown in Table 1, processes 1–5 and 9–11, are used. The enzyme rate equations are given in [20]. The theoretical curves were computed with SCAMP (see theoretical methods) using the parameter values of Table 3 (this study) and Table 1 in [20]. Metabolites: ◆, aspartate (asp); □, β-aspartyl phosphate + *O*-phospho-homoserine (aspp + hsp); △, aspartic β-semialdehyde (asa); ◇, homoserine (hs); ■, threonine (thr). Co-metabolites: ○, NADPH; ●, ATP. The continuous curves represent the model simulation results. Initial concentrations for variable aspartate: 2 mM NADPH, 5 mM ATP, no threonine and (**a**) 0.5 mM, (**b**) 2 mM or (**c**) 5 mM aspartate. Initial concentrations for variable threonine: 2 mM NADPH, 10 mM ATP, 2 mM aspartate and (**d**) 0 mM, (**e**) 0.5 mM or (**f**) 2 mM threonine.

criteria, the first two enzymes should be classed as near-equilibrium steps. In case this was a peculiarity of the Tir-8 strain, the calculation was repeated with 10-fold lower levels of aspartate kinase I and homoserine dehydrogenase I, as an approximation to the relative enzyme activities of a wild-type cell. This resulted in the first two enzymes moving closer to

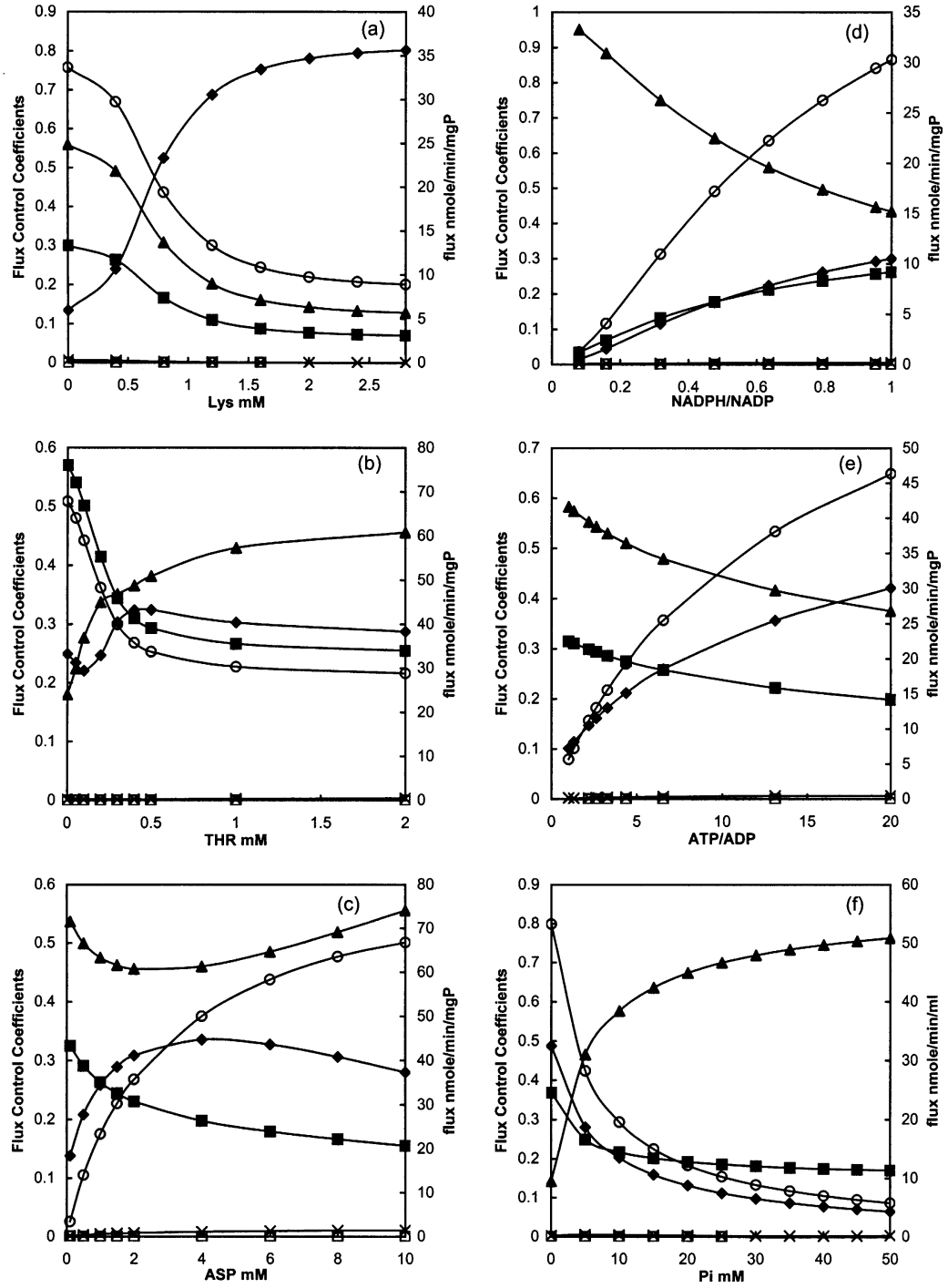

Figure 3 Responses of the *in vivo* simulations to external metabolites

The dependencies on external metabolite concentrations of the flux control coefficients of the five steps of the threonine pathway and the threonine-synthesis flux were computed for the *in vivo* conditions of Table 5, except for the metabolites varied as indicated on the abscissae. Symbols/lines: ◆, C^J_{AK}; ■, C^J_{ASADH}; ▲, C^J_{HDH}; ×, C^J_{HK}; □, C^J_{TS}; ○, threonine flux, J (for enzyme abbreviations see Figure 1). Note that, in this figure, the symbols are used solely to differentiate the curves; many more points were simulated to construct the curves.

equilibrium and the third moving away, with values of 0.93, 0.93 and 4.2×10^{-5} respectively.

Prediction of flux control coefficients *in vivo*

At the steady state simulated in the previous section for *in vivo* conditions, SCAMP was used to compute the control coefficients by perturbation of the limiting rates of each of the reactions. In the case of aspartate kinase, a dummy parameter was used to modulate the two components in parallel, so that a single flux control coefficient was obtained for the step, although this of course is the sum of two contributions from each of the isoenzymes in the model. The results are presented in Table 5. It

Table 5 Predicted flux control coefficients of the threonine-synthesis pathway *in vivo*

Enzyme	Flux control coefficient	Flux control coefficient at 0 mM threonine
Aspartate kinase	0.28	0.249
Aspartate semialdehyde dehydrogenase	0.25	0.57
Homoserine dehydrogenase	0.465	0.18
Homoserine kinase	0.005	0.002
Threonine synthase	0.0	0.0

can be seen that the control of flux is shared between the first three enzymes of the pathway, with most control on the third step, homoserine dehydrogenase. It is notable that the two enzymes that are essentially irreversible (homoserine kinase and threonine synthase) have essentially no flux control, whereas two enzymes that are relatively near equilibrium (aspartate kinase and aspartate semialdehyde dehydrogenase) together have over half the flux control in the pathway. Classical theories of metabolic regulation assume that a pathway will be controlled by feedback inhibition on a 'committed' (i.e. irreversible) step [11], but these results show that aspartate kinase is not a committed step and is not strongly controlling, even though feedback-inhibited by threonine and lysine. On the other hand, homoserine dehydrogenase is the first step after the pathway to lysine branches from the threonine–methionine–isoleucine pathway, and it is a conventional committed, feedback-inhibited step with significant potential for flux control.

It should be emphasized that these results almost certainly give larger values for the flux control coefficients of the threonine-pathway enzymes than would be measured on whole cells. This is because the simulations have considered the pathway as an isolated unit, whereas the supply of aspartate and the removal of threonine for protein synthesis (and by diffusion out of the cell) also potentially have some control. This is investigated below.

The exact values of the flux control coefficients do depend on the assumed levels of the amino acids aspartate, threonine and lysine, although a consistent feature over a wide range of conditions is the distribution of the control between the first three enzymes, with no single one becoming a dominating controlling factor (Figure 3). The concentration of threonine might rightly be expected to have an influence since it is an effector of the first, third and fourth steps (Figure 1), of which the first two have appreciable control coefficients. (Indeed, the total response of the pathway to threonine will be the sum of the responses from each enzyme to threonine, in each case composed of the product of the enzyme's flux control coefficient and its elasticity towards threonine, as shown in eqn 5.) In addition, the concentration of free threonine might be expected to be higher in this constitutive threonine producer than in a wild-type cell. Nevertheless, the third column of Table 5 shows that even with no free threonine the control is distributed over the first three steps, although the removal of threonine inhibition on aspartate kinase and homoserine dehydrogenase has lowered their flux control coefficients, which is the expected consequence of increasing the activity of an enzyme in a pathway under normal circumstances [4,6,10,11]. Repeating the calculation at various threonine concentrations shows that threonine has inhibited the pathway flux almost as far as it is able by 0.5 mM (Figure 3b), and at that point the distribution of flux control is almost the same as that shown in the second column of Table 5.

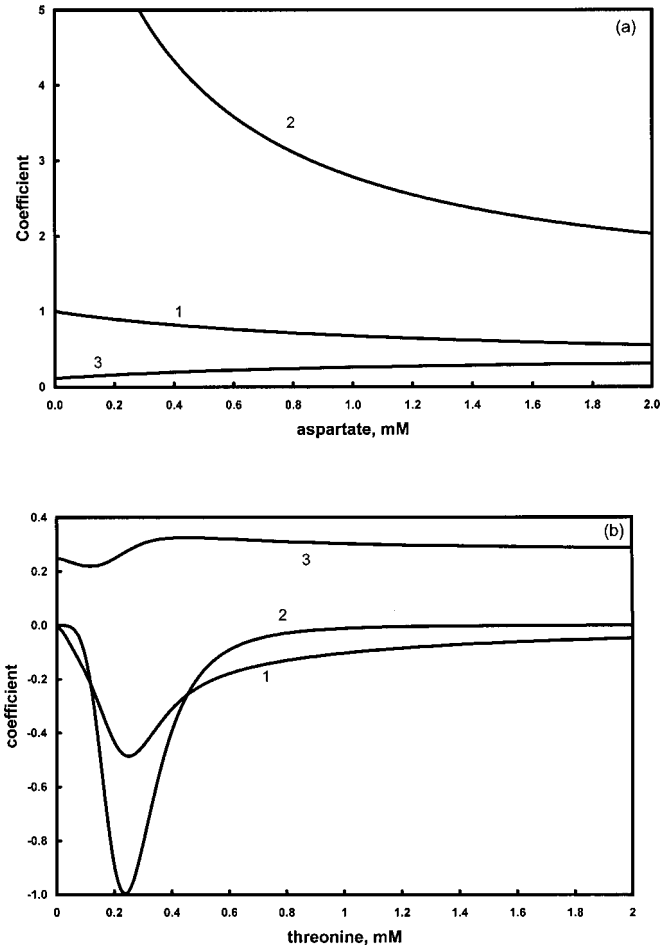

Figure 4 Response coefficients of the threonine flux to aspartate and threonine

(**a**) Aspartate variable (Figure 3c): curve 1, R^J_{Asp}; curve 2, ϵ^{AK}_{Asp}; curve 3, C^J_{AK}. (**b**) Threonine variable (Figure 3b): curve 1, R^J_{Thr}; curve 2, ϵ^{AK}_{Thr}; curve 3, C^J_{AK}. AK, aspartate kinase.

The other feedback inhibitor of the pathway is lysine, an effector of aspartate kinase and homoserine kinase. As lysine increases, the flux control coefficient of homoserine dehydrogenase falls and that of aspartate kinase rises, until at approx. 0.7 mM lysine, aspartate kinase has the largest flux control coefficient (Figure 3a). Again, the increase in the flux control coefficient of aspartate kinase is the expected result of the inhibition of its activity. Since all the flux control coefficients together always add up to 1, according to the summation theorem for flux control coefficients [9–11], the increase in this enzyme's flux control coefficient has to be compensated by an equivalent reduction in control by the other enzymes, and in this case the change is at the expense of homoserine dehydrogenase.

Our experimental study of the pathway dynamics [21] showed that the pathway appeared more sensitive to aspartate than to threonine concentrations. This is also seen in the simulations of the steady state (Figure 3c). A more precise measure of the relative sensitivities to aspartate and threonine is given by the response coefficients of the flux with respect to these two amino acids (Figure 4). For aspartate concentrations up to 2 mM, at fixed threonine, the response coefficient of the flux to aspartate always lies between 0.5 and 1, where a value of 1 would correspond to a proportional response of the flux to aspartate.

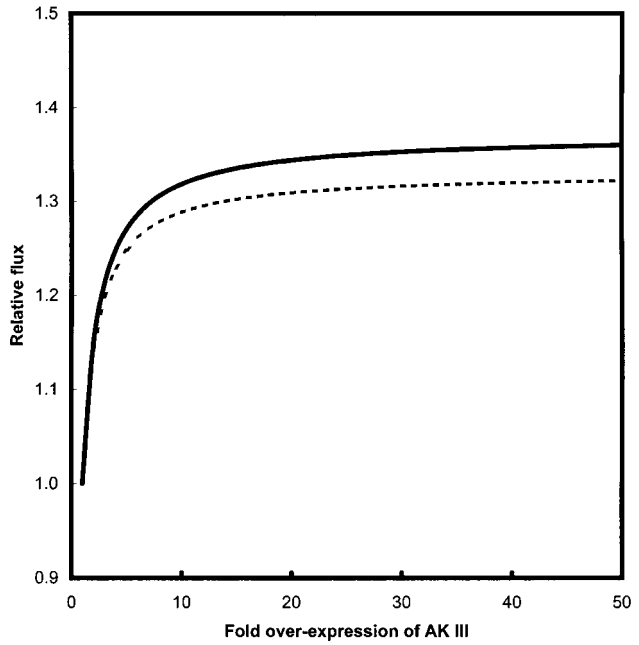

Figure 5 Over-expression of aspartate kinase III (AK III)

Solid line, simulated steady-state flux for conditions *in vivo* in *E. coli* Tir-8 relative to the flux and enzyme activity in wild-type cells. Dashed line, prediction of flux change using eqn (7).

For threonine over the same concentration range at fixed aspartate, the response coefficient becomes −0.5 at 0.25 mM threonine (where the negative value indicates that threonine is inhibiting the flux). It may seem surprising that the response to aspartate, which acts only on aspartate kinase, is always larger than the step's flux control coefficient. The reason is that response coefficients are the products of flux control coefficients and elasticities [9] (see also eqn 5), and the composite elasticity of the total aspartate kinase to aspartate is greater than 2, rising to 8 and beyond at low aspartate concentrations. This large elasticity is because the aspartate kinase step is close to equilibrium, as described above, and near-equilibrium enzymes invariably exhibit a great sensitivity of the net rate to their substrate and product concentrations [9,11]. Hence this is an interesting example of a case where the strong response of the pathway to the pathway substrate cannot be interpreted as indicating rate limitation by the first step. In the case of the response to threonine, the response is the sum of the responses of each of the enzymes for which threonine is an effector, as discussed above. Figure 4 shows only the components of the aspartate kinase response: the flux control coefficient of that step and its elasticity to threonine. At 0.25 mM, aspartate kinase contributes about half the pathway response to threonine, and it can be seen that the variability in response with different threonine concentrations is a result of the concentration dependence of this elasticity. Thus in spite of its relatively small flux control coefficient, aspartate kinase is still responsible for much of the pathway's response to aspartate and threonine.

Figure 3 also shows the responses of the flux and flux control coefficients of the model to the assumed values of the NADPH/NADP$^+$ and ATP/ADP ratios and the concentration of inorganic phosphate. Although the results are sensitive to the values of these parameters, it can be seen that even if there are uncertainties in the measured values, reported in Table 4, they would not affect our conclusions substantially.

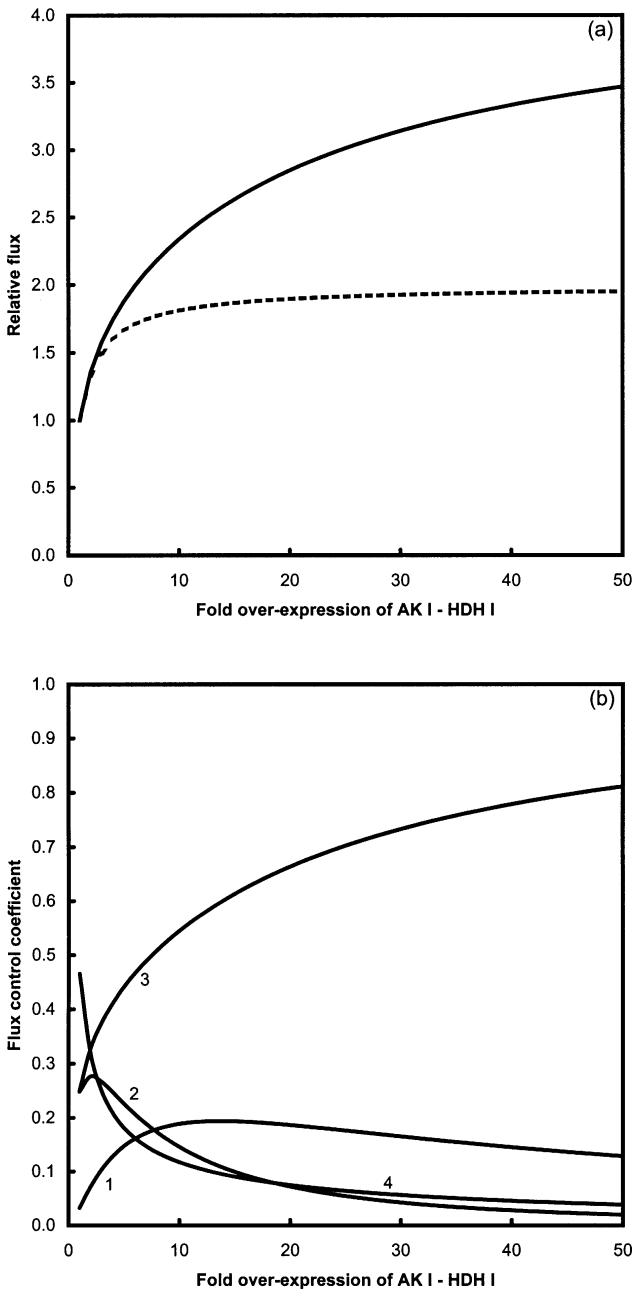

Figure 6 Over-expression of aspartate kinase I (AK I)/homoserine dehydrogenase I (HDH I)

(**a**) Solid line, simulated steady-state flux for *in vivo* conditions in *E. coli* Tir-8 relative to the flux and enzyme activity in wild-type cells. Dashed line, prediction of flux change using eqn (7). (**b**) Flux control coefficients of the threonine-pathway enzymes: curve 1, aspartate kinase I; curve 2, aspartate kinase III; curve 3, aspartate semialdehyde dehydrogenase; curve 4, homoserine dehydrogenase. Not shown: homoserine kinase and threonine synthase.

Prediction of the effects of over-expressing pathway enzymes

By using the model-control facilities in the simulator SCAMP, the effects of specifically over-expressing an enzyme on the steady state of the pathway can be simulated under the *in vivo* conditions used in the previous section. An implicit assumption in this approach is that the over-expression has an effect neither on the boundary metabolites (aspartate, threonine, NADPH/NADP$^+$

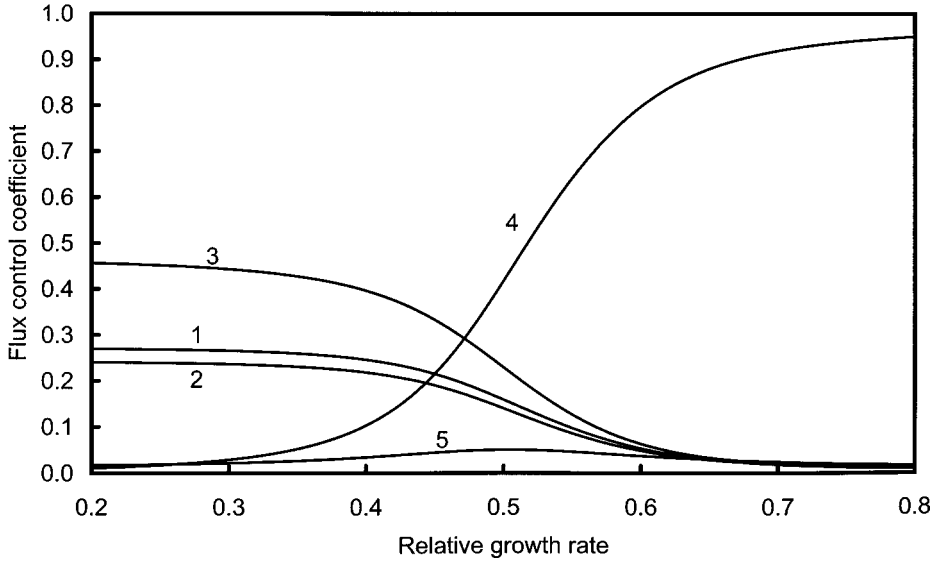

Figure 7 Effect of threonine demand on the flux control coefficients of the threonine pathway

The control coefficients are calculated for the steady states of the extended model of Figure 1 for a range of growth rates, expressed as a fraction of the maximal growth rate. Flux control coefficients: curve 1, total aspartate kinase; curve 2, aspartate semialdehyde dehydrogenase; curve 3, homoserine dehydrogenase; curve 4, all protein-synthesis steps from threonine (threonyl-tRNA synthetase, threonine deaminase, out1 and out2 in Figure 1); curve 5, threonine leak from the cells.

and ATP/ADP) nor on the expression levels of the other enzymes. Obviously this assumption will be less tenable if the model predicts over-expression to have a significant impact on the pathway. Two cases are examined here. In the first, aspartate kinase III was over-expressed up to 50 times its normal level in *E. coli* Tir-8. For these simulations, the two aspartate kinases have to be treated separately and assigned individual flux control coefficients, in effect as two reactions converging on β-aspartyl phosphate. In spite of the large change in enzyme content, the predicted flux increase is less than 40% (Figure 5), and this change can be approximately predicted from the initial flux control coefficient of aspartate kinase III using Small and Kacser's finite-change formula ([4] and eqn 7). Evidently this supports the arguments from metabolic control analysis [4–6,36] that over-expression of a single enzyme has limited potential for causing large flux changes. It is also consistent with observations in other organisms, admittedly with different control structures, i.e. *Saccharomyces cerevisiae* [37,38] and *C. glutamicum* [39–41], that the activation of aspartate kinase (often by mutation to a feedback-resistant form) is necessary, but not sufficient without other alterations to the pathway, to give significant threonine production.

When the over-expression of aspartate kinase I is simulated, it is also necessary to increase the activity of homoserine dehydrogenase I in parallel, since this is a bifunctional enzyme. Figure 6(a) shows that this results in a much larger increase in the flux, 3.5-fold for a 50-fold increase in enzyme activity. This is not solely because aspartate kinase I and homoserine dehydrogenase together have a larger flux control coefficient than either of the aspartate kinase isoenzymes: the effect that a larger flux control coefficient of the amplified unit will have on the flux response can be calculated with eqn (7) as before, but using the combined control coefficient, and it can be seen that the prediction is for a less than 2-fold increase. The explanation for this underestimate by the finite-change formula relative to the simulated results can be seen by examining the effect of the enzyme increase on the flux control coefficients (Figure 6b). Even though aspartate kinase I is being over-expressed, at first its flux control coefficient (and that of aspartate kinase III) starts to increase, apparently paradoxically. This is because the fall in the control coefficient of homoserine dehydrogenase I as aspartate kinase I is over-expressed is more significant, and, since the flux summation theorem [9] requires that the sum of the flux control coefficients remains at unity, the control lost by this enzyme is necessarily transferred to the other enzymes, including the aspartate kinases. This effect does not occur in the case of over-expression of aspartate kinase III, where the flux control coefficients of both aspartate kinases fall monotonically as the level of expression increases (results not shown).

Effects of threonine demand on simulated threonine synthesis

A potential weakness in the previous results is that the predictions assume constant levels of threonine, and hence are responsive neither to variations in the demand for threonine nor in the overall rate of its supply. We therefore extended the model as used for the previous simulations to include use of threonine for protein synthesis, both directly and via isoleucine, and to allow excess threonine to diffuse from the cell (Figure 1). In these new simulations, threonine is no longer a fixed parameter but a free variable. The demand for threonine can be varied by changing the assumed growth rate. Although these extra steps do not have such a sound empirical base as the steps of the main pathway, they are sufficient to assess the sensitivity of the conclusions reached with the core model to this additional factor.

Figure 7 shows how the distribution of the flux control coefficients changes with growth rate, where the growth rate is expressed as a fraction of that exhibited by wild-type *E. coli*. It can be seen that at low growth rates, the control is largely in the threonine pathway itself, and it is only at higher growth rates that the demand for threonine comes to dominate the control of the threonine synthesis rate. As far as the control of threonine

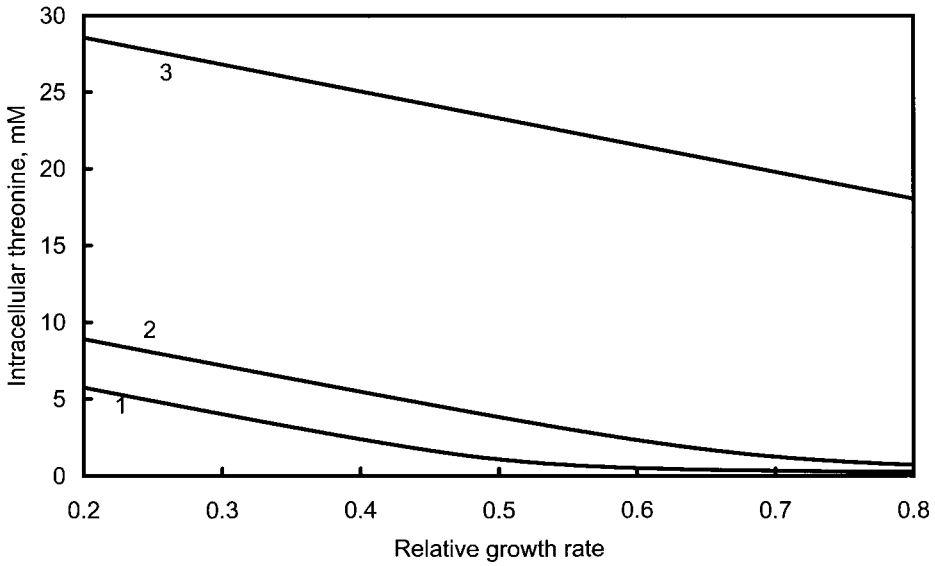

Figure 8 Accumulation of threonine at different growth rates

For the full model, with growth-dependent threonine demand included, the simulated concentration of intracellular threonine is plotted for the control Tir-8 strain (curve 1) and cells with 50-fold over-expression of aspartate kinase III (curve 2) or aspartate kinase I/homoserine dehydrogenase I (curve 3).

synthesis by enzymes of the synthetic pathway is concerned, the distribution of control between them, as represented by their relative flux control coefficients, is not altered by changing demand. It is the total amount of control exerted by the synthetic enzymes that decreases as the demand for threonine is increased. Hence the conclusions reached by simulating just the five steps of the synthetic pathway are broadly correct, although the actual values of the flux control coefficients might be over-estimated.

Figure 8 shows that low growth rates lead to a tendency to accumulate and excrete threonine, because even at high threonine levels the synthesis is not completely inhibited. Here the simulations reflect a common feature of microbial amino acid production: free amino acids generally tend to accumulate only as the cells start to pass into the stationary phase. The leak of threonine from the cell is the only exception to the gradual monotonic exchange of control between the synthesis steps and the demand steps; it rises to a maximum of approx. 0.05 at the cross-over in control between synthesis and demand and then falls again (Figure 7).

Figure 8 also demonstrates that there is markedly higher accumulation of threonine when the aspartate kinases are over-expressed; even though the overall effects of over-expression on the threonine-synthesis flux were not so large, the effects on threonine export and intracellular threonine concentration were proportionately much more significant. The simulated threonine concentrations at low growth rate are comparable with the intracellular concentrations in threonine-producing strains of *C. glutamicum* [39].

Conclusions

This study has shown that the measured kinetics of the enzymes of the threonine pathway, as described in the first paper of this series [20], can form the basis of an adequate representation of a threonine-synthesizing system *in vitro*. Furthermore, it does not seem essential to use mechanistically exact kinetic equations, since our simplified equations performed adequately. Since the flux predicted by the model at steady state, with estimated *in vivo* levels of the external metabolites, is close to that required to support growth of the bacterium, it seems unlikely that there are major effectors in the cell that are unaccounted for in the model, which can therefore be used as a guide to the functioning of the pathway *in vivo*. As far as this pathway is concerned, there seems to be no reason to doubt that the cell is just a bag of enzymes. On this basis, it would be worthwhile extending the model to include the reactions leading to other amino acids of the aspartate group, and to consider developing an equivalent for *C. glutamicum*, which is the favoured organism for industrial production of several of these amino acids, and for which a model of the partially overlapping lysine pathway already exists [18].

The simulated results underline an important feature of the pathway that is not represented correctly in most accounts of it in textbooks and elsewhere. In terms of the reactions catalysed and their equilibrium constants, the first two reactions of the threonine pathway are close analogues of phosphoglycerate kinase and glyceraldehyde-3-phosphate dehydrogenase in the glycolytic pathway, except that the direction of threonine synthesis corresponds to the gluconeogenic direction. Accordingly, it would be expected that the first two reactions of threonine synthesis are reversible, and this is what the simulations confirm, with both reactions being close to equilibrium under all conditions examined. Invariably though, the pathway is shown as if both these reactions are irreversible in the threonine direction, presumably to accord with the prevailing dogma that feedback inhibition occurs on the first committed step of a pathway. Thus the study of this pathway demonstrates that feedback-inhibition mechanisms can occur on near-equilibrium steps, and it also provides two instances of enzymes that are close to equilibrium yet have finite flux control coefficients. Nevertheless, the flux control coefficient of aspartate kinase is weak, which perhaps explains why modulation of this enzyme alone, in *C. glutamicum*, has not been sufficient to increase flux to threonine or lysine greatly (although the regulatory structure of the pathway differs in this organism from that in *E. coli*).

We thank the company Eurolysine and the région Aquitaine for supporting this work. D. A. F. was appointed as an invited professor by the University Bordeaux 2 during this work.

REFERENCES

1 Nielsen, J. (1998) Metabolic engineering: techniques for analysis of targets for genetic manipulations. Biotechnol. Bioeng. **58**, 125–132
2 Cremer, J., Eggeling, L. and Sahm, H. (1991) Control of the lysine biosynthesis sequence in *Corynebacterium glutamicum* as analyzed by over-expression of the individual corresponding genes. Appl. Environ. Microbiol. **57**, 1746–1752
3 Cornish-Bowden, A., Hofmeyr, J.-H. S. and Cárdenas, M. L. (1995) Strategies for manipulating fluxes in biotechnology. Bioorg. Chem. **23**, 439–449
4 Small, J. R. and Kacser, H. (1993) Responses of metabolic systems to large changes in enzyme activities and effectors. 1. The linear treatment of unbranched chains. Eur. J. Biochem. **213**, 613–624
5 Kacser, H. and Acerenza, L. (1993) A universal method for achieving increases in metabolite production. Eur. J. Biochem. **216**, 361–367
6 Fell, D. A. (1998) Increasing the flux in metabolic pathways: a metabolic control analysis perspective. Biotechnol. Bioeng. **58**, 121–124
7 Niederberger, P., Prasad, R., Miozzari, G. and Kacser, H. (1992) A strategy for increasing an *in vivo* flux by genetic manipulation: the tryptophan system of yeast. Biochem. J. **287**, 473–479
8 Patnaik, R., Spitzer, R. G. and Liao, J. C. (1995) Pathway engineering for production of aromatics in *Escherichia coli*: confirmation of stoichiometric analysis by independent modulation of arog, tkta and pps activities. Biotechnol. Bioeng. **46**, 361–370
9 Kacser, H. and Burns, J. A. (1973) The control of flux. Symp. Soc. Exp. Biol. **27**, 65–104; reprinted (1995) in Biochem. Soc. Trans. **23**, 341–366
10 Fell, D. A. (1992) Metabolic control analysis: a survey of its theoretical and experimental developments. Biochem. J. **286**, 313–330
11 Fell, D. A. (1997) Understanding the Control of Metabolism, Portland Press, London
12 Heinrich, R. and Rapoport, T. A. (1974) A linear steady-state treatment of enzymatic chains; general properties, control and effector strength. Eur. J. Biochem. **42**, 89–95
13 Reder, C. (1988) Metabolic control theory: a structural approach. J. Theor. Biol. **135**, 175–201
14 Stephanopoulos, G. and Simpson, T. W. (1997) Flux amplification in complex metabolic networks. Chem. Eng. Sci. **52**, 2607–2627
15 Theilgaard, H. B. A. (1999) Quantification and kinetic analysis of the penicillin biosynthetic pathway in *Penicillium chrysogenum*. PhD thesis, Technical University of Denmark
16 Kholodenko, B. N., Cascante, M., Hoek, J. B., Westerhoff, H. V. and Schwaber, J. (1998) Metabolic design: how to engineer a living cell to desired metabolite concentrations and fluxes. Biotechnol. Bioeng. **59**, 239–247
17 Thomas, S., Mooney, P. J. F., Burrell, M. M. and Fell, D. A. (1997) Metabolic control analysis of glycolysis in tuber tissue of potato (*Solanum tuberosum*). Explanation for the low control coefficient of phosphofructokinase over respiratory flux. Biochem. J. **322**, 119–127
18 Yang, C., Hua, Q. and Shimizu, K. (1999) Development of a kinetic model for L-lysine biosynthesis in *Corynebacterium glutamicum* and its application to metabolic control analysis. J. Biosci. Bioeng. **88**, 393–403
19 Xiu, Z. L., Zeng, A. P. and Deckwer, W. D. (1997) Model analysis concerning the effects of growth rate and intracellular tryptophan level on the stability and dynamics of tryptophan biosynthesis in bacteria. J. Biotechnol. **58**, 125–140
20 Chassagnole, C., Raïs, B., Quentin, E., Fell, D. A. and Mazat, J.-P. (2001) An integrated study of threonine-pathway enzyme kinetics in *Escherichia coli*. Biochem. J. **356**, 415–423
21 Raïs, B., Chassagnole, C., Letellier, T., Fell, D. A. and Mazat, J.-P. (2001) Threonine synthesis from aspartate in *Escherichia coli* cell-free extracts: pathway dynamics. Biochem. J. **356**, 425–432
22 Cayley, S., Lewis, B. A. and Record, M. (1992) Origins of the osmoprotective properties of betaine and proline in *Escherichia coli* K-12. J. Bacteriol. **174**, 1586–1595
23 Joseph, M. H. and Marsden, C. A. (1986) Amino acids and small peptides. In HPLC of Small Molecules, a Practical Approach (Lim, C. K., ed.), pp. 13–28, IRL Press, Oxford
24 Wulff, K. and Doppen, W. (1985) ATP: luminometric method. In Methods of Enzymatic Analysis, vol. 7 (Bergmeyer, H. U., ed.), pp. 357–364, VCH Verlagsgesellschaft, Weinheim
25 Hampp, R. (1985) ADP, AMP: luminometric method. In Methods of Enzymatic Analysis, vol. 7 (Bergmeyer, H. U., ed.), pp. 370–379, VCH Verlagsgesellschaft, Weinheim
26 Lilius, E., Multanen, V. and Toivonen, V. (1979) Quantitative extraction and estimation of intracellular nicotinamide nucleotides of *Escherichia coli*. Anal. Biochem. **99**, 22–27
27 Wimpenny, J. W. T. and Firth, A. (1972) Levels of nicotinamide adenine dinucleotide and reduced nicotinamide adenine dinucleotide in facultative bacteria and the effect of oxygen. J. Bacteriol. **111**, 24–32
28 Cayley, S., Lewis, B. A., Guttman, H. and Record, M. (1991) Characterization of the cytoplasm of *Escherichia coli* K12 as a function of external osmolarity, implications for protein DNA interactions *in vivo*. J. Mol. Biol. **222**, 281–300
29 Neidhardt, F. C. (1996) *Escherichia coli* and *Salmonella*. Molecular and Cellular Biology, ASM Press, Washington DC
30 Holmes, W. H. (1986) The central metabolic pathways of *Escherichia coli*: relationship between flux and control at a branch point, efficiency of conversion to biomass, and excretion of acetate. Curr. Top. Cell. Regul. **28**, 69–105
31 Palmieri, L., Berns, D., Kramer, R. and Eikmanns, M. (1996) Threonine diffusion and threonine transport in *Corynebacterium glutamicum* and their role in threonine production. Arch. Microbiol. **165**, 48–54
32 Snell, K. and Fell, D. A. (1990) Metabolic control analysis of mammalian serine metabolism. Adv. Enzyme Regul. **30**, 13–32
33 Sauro, H. M. (1993) SCAMP: a general-purpose simulator and metabolic control analysis program. Comput. Appl. Biosci. **9**, 441–450
34 Black, S. and Wright, N. G. (1955) Aspartic β-semialdehyde dehydrogenase and aspartic β-semialdehyde. J. Biol. Chem. **213**, 39–50
35 Patte, J.-C., Truffa-Bachi, P. and Cohen, G. N. (1966) The threonine-sensitive homoserine dehydrogenase and aspartokinase activities of *Eschersichia coli*. 1. Evidence that the two activities are carried by a single protein. Biochim. Biophys. Acta **128**, 426–439
36 Fell, D. A. and Thomas, S. (1995) Physiological control of flux: the requirement for multisite modulation. Biochem. J. **311**, 35–39
37 Farfán, M.-J., Aparicio, L. and Calderón, I. L. (1999) Threonine overproduction in yeast strains carrying the *hom3-r2* mutant allele under the control of different inducible promoters. Appl. Environ. Microbiol. **65**, 110–116
38 Farfán, M.-J. and Calderón, I. L. (2000) Enrichment of threonine content in *Saccharomyces cerevisiae* by pathway engineering. Enzyme Microb. Technol. **26**, 763–770
39 Kronemeyer, W., Eggeling, L., Eikmanns, B. J. and Sahm, H. (1994) Stable expression of *hom-1-thrb* in *Corynebacterium glutamicum* and its effect on the carbon flux to threonine and related amino acids. Appl. Environ. Microbiol. **60**, 126–132
40 Colón, G. E., Jetten, M. S. M., Nguyen, T. T., Gubler, M. E., Follettie, M. T., Sinskey, A. J. and Stephanopoulos, G. (1995) Effect of inducible *thrb* expression on amino acid production in *Corynebacterium lactofermentum* ATCC 21799. Appl. Environ. Microbiol. **61**, 74–78
41 Eggeling, L., Morbach, S. and Sahm, H. (1997) The fruits of molecular physiology: engineering the L-isoleucine biosynthesis pathway in *Corynebacterium glutamicum*. J. Biotechnol. **56**, 167–182

Received 6 October 2000/2 January 2001; accepted 5 March 2001